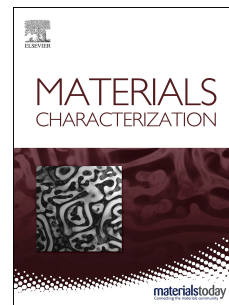# Journal Pre-proof

Fracture toughness characteristics of ultrafine grained Nb–Ti stabilized microalloyed and interstitial free steels processed by advanced multiphase control rolling

Sumit Ghosh, Suhrit Mula

Please cite this article as: S. Ghosh, S. Mula, Fracture toughness characteristics of ultrafine grained Nb–Ti stabilized microalloyed and interstitial free steels processed by advanced multiphase control rolling, *Materials Characterization* (2019), doi: https://doi.org/10.1016/j.matchar.2019.110003.

This is a PDF file of an article that has undergone enhancements after acceptance, such as the addition of a cover page and metadata, and formatting for readability, but it is not yet the definitive version of record. This version will undergo additional copyediting, typesetting and review before it is published in its final form, but we are providing this version to give early visibility of the article. Please note that, during the production process, errors may be discovered which could affect the content, and all legal disclaimers that apply to the journal pertain.
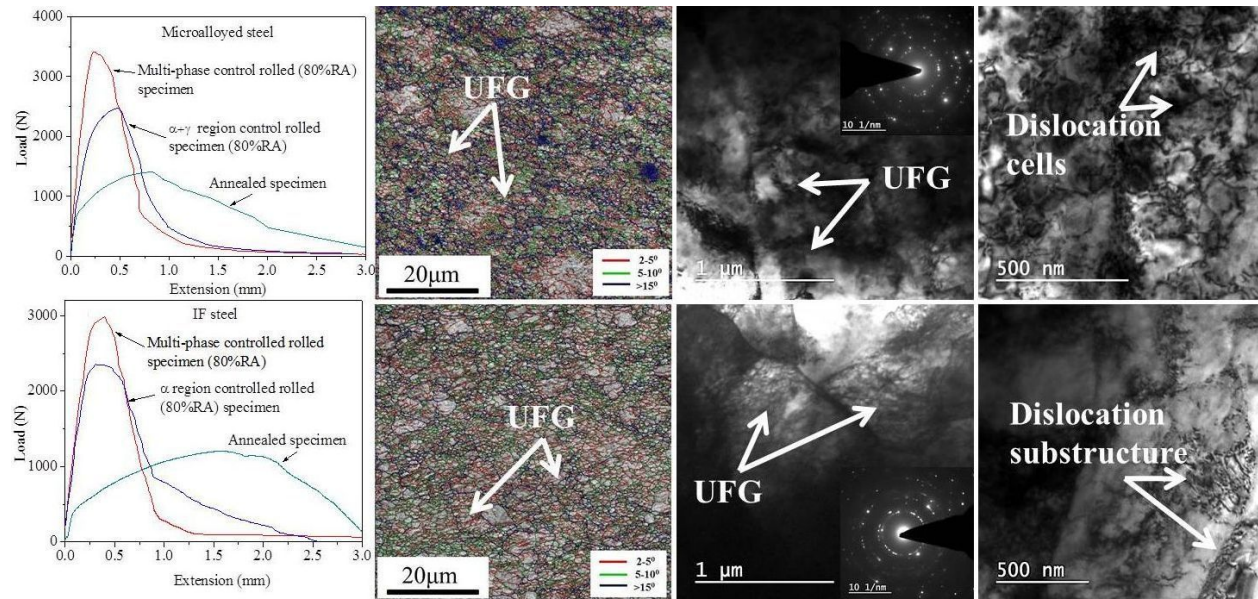
Fracture toughness characteristics of ultrafine grained Nb-Ti stabilized microalloyed and interstitial free steels processed by advanced multiphase control rolling

Sumit Ghosh[a,b], Suhrit Mula[b]*

[a] Materials and Mechanical Engineering, Centre for Advanced Steels Research, University of Oulu, 90014 Oulun yliopisto, Finland.

[b] Department of Metallurgical and Materials Engineering, Indian Institute of Technology Roorkee, Roorkee-247667, Uttarakhand, India.

*Corresponding Author: Email: smulafmt@iitr.ac.in, suhritmula@gmail.com

Phone: +91-1332-285763; Fax: +91-1332-285243

Abstract

Aim of the current study is to analyze the fracture toughness values along with other mechanical properties and correlating the microstructures of ultrafine grained (UFG) microalloyed and interstitial free (IF) steels produced through advanced 3-steps control multiphase rolling. The analysis of fracture toughness was carried out through computing K_Q (conditional fracture toughness), J-integral (crack initiation energy) and K_{ee} (equivalent energy fracture toughness) values from 3-point bend test data of rolled specimens. Microstructural analysis was performed through transmission electron microscopy (TEM) along with selected area electron diffraction (SAED) and Electron backscatter diffraction (EBSD). The quantitative measurement of low and high angle grain boundaries and their distribution in the deformed state were determined through EBSD analysis. The good combinations of fracture toughness, yield strength (YS) and percent elongation (%El.) (i.e. ductility) were achieved through innovative 3-phase control rolling (microalloyed steel: K_{ee}=68.9MPa√m, J=81.4kJ/m^2, YS=923MPa, %El.=13.6; IF steel: K_{ee}=72MPa√m, J=87.7kJ/m^2, YS=623Mpa and %El.=19). This is ascribed to the development of homogeneously distributed submicron size (0.69µm) ferritic+martensitic structure in the microalloyed steel and submicron size (0.83µm) ferritic grains along with high density dislocation substructure in the IF steel. These dislocation cells and substructures could effectively block the crack initiation and propagation. The development of UFG microstructure has been analyzed in the light of deformation induced ferrite transformation (DIFT) and dynamic recrystallization (DRX) mechanisms. Superior fracture toughness of the UFG steels along with better combination of mechanical properties is very demanding for high strength structural applications.

1. Introduction

Demand of enhancement of the surviving strength of the microalloyed/interstitial free (IF) steels is raised steadily to improve the performance of the structural components. Improving yield strength of the steels without much sacrificing their toughness and ductility is a challenge practically. Grain refinement is one of the most promising techniques by which the strength and toughness can be improved simultaneously [1,2]. Thermomechanical control rolling (TMCR) methods are extensively carried out due to their capability to refine the grain size of metals and its alloys without much deteriorating its toughness [3,4]. The maximum grain refinement (grain size 1-3µm) during rolling at intercritical region for the microalloyed steel is attributed to both deformation induced ferrite transformation (DIFT) of austenite into ferrite and dynamic recrystallization (DRX) of the ferrite [2]. Moreover, warm-rolling of the IF steel in ferritic region could also produce a fine ferritic structure (grain size 2-5µm) through DRX [5]. Overall, DIFT and DRX are two key mechanisms to achieve fine ferrite grains in the steels, which could provide a good combination of yield strength, ductility and toughness [5,6]. But, unfortunately, through conventional rolling method, the ferrite grain refinement has reached its limitation within several micrometers (2-4µm) even after employing high strain deformation [7,8]. Although, some authors [9,10] reported to achieve very fine ferrite grains (1-2µm) through conventional DIFT mechanism through application of extremely high-strain deformation (~80% deformation in a single pass), this would exceed the capability of most of the industrial TMCR facilities. Recently, some authors [11,12] recommended that DRX could occur in the deformation induce transformed ferrite, which may bring about further refinement of ferrite grains to <1µm and the materials could exhibit good combination of mechanical properties by means of microstructural refinement.

Furthermore, ultrafine grained (UFG) materials produced through advanced TMCR techniques although offer exceptional mechanical properties, the deformation characteristics may be deteriorated due to the reduced strain hardening response. Thus, investigation of fracture toughness is extremely crucial prior to any design applications, as this would provide more detail

information about the deformation features and fracture activities of such ultrafine grained (UFG) materials [13]. The fracture toughness testing of the UFG steels is challenging; hence, hardly any data is available about the valid K_{IC} (plane strain fracture toughness) of the UFG materials due to the limited specimen dimension (especially thickness) obtained through advance thermomechanical control processing. Recently, Dashrath et al. [14], Joshi et al. [15] and Toulfatzis et al. [16] made an effort to evaluate the fracture toughness values by 3-point bend tests and reported that the grain size refinement has significant effect on the improvement of conditional fracture toughness of nonferrous UFG materials developed through cryorolling/cryoforging techniques. Recently, the uses of microalloyed and IF steels have been expanded in several sectors, such as, ship building, automotive, line pipe and several structural applications. Thus, the materials must have high fracture toughness properties to use these materials with enhanced performance for such applications. Therefore, aim of the current study is to design advanced TMCR schedules in order to achieve microalloyed and IF steels with submicron sized grains (<1µm), which could provide high fracture toughness values along with good combination of yield strength and ductility. Hence, in the present study, single and 3-steps multiphase control thermomechanical processing schedules have been designed with an aim to achieve UFF grains <1µm. Furthermore, the analysis of fracture toughness was carried out through computing K_Q, K_{ee} and J-integral values obtained through analysing the 3-point bend test results of control rolled specimens (UFG samples) and correlated with microstructure and other mechanical properties.

2. Materials and detail experimental methods

Detail chemical compositions (wt.%) acquired through optical emission spectroscopy analysis of the IF and microalloyed (MA) steels are shown in Table 1.

Table 1: Chemical compositions (wt.%) of the IF and microalloyed steels.

Elements (wt.%)	C	Mn	Al	Si	Nb	Ti	P	S	N	Fe
IF steel	0.003	0.14	0.052	0.007	0.012	0.042	0.031	0.008	0.002	99.7
MA steel	0.11	1.44	0.01	0.344	0.044	0.028	0.016	0.003	0.01	97.92

Single and multiphase control rolling have been conducted using a 4-high rolling mill with the aim to obtain UFG microalloyed/IF steels having significant amount of formability and good

fracture toughness. The specimens with dimensions of 55×45×30mm were machined from the as received steels. In order to achieve a uniform microstructure and dissolve all the microalloying elements, i.e. Nb and Ti, all the specimens were first homogenized at 1200°C for 1h; afterwards the samples were compressed at the chosen temperatures. Prior to design the deformation schedules, Ar$_3$/Ar$_1$ temperatures were evaluated through dilatometric analysis using Gleeble-3800 thermomechanical simulator. In this case, the specimen (6mm diameter and 80mm length) was first heated up to austenitization temperature (1200°C) at a rate of 5°Cs^{-1}, and then holding for 2min at 1200°C followed by cooling to room temperature at a rate of 1°Cs^{-1}. Ar$_3$ and Ar$_1$ are estimated to be 750 & 685°C, respectively, for the microalloyed steel, and 880 & 820°C, respectively, for the IF steel. Firstly, single phase control rolling was conducted at intercritical (α+γ) and pure ferritic (α) phase regime at ~700°C and ~650°C for microalloyed and IF steels, respectively, followed by water quenched (WQ) to room temperature (as shown schematically in Fig. 1a and b). Total 4 and 8 numbers of hits were given to attain total reduction in area (RA) 50 and 80% (equivalent true strain 0.7 and 1.6) in both the steels, respectively at a strain rate 0.1/s.
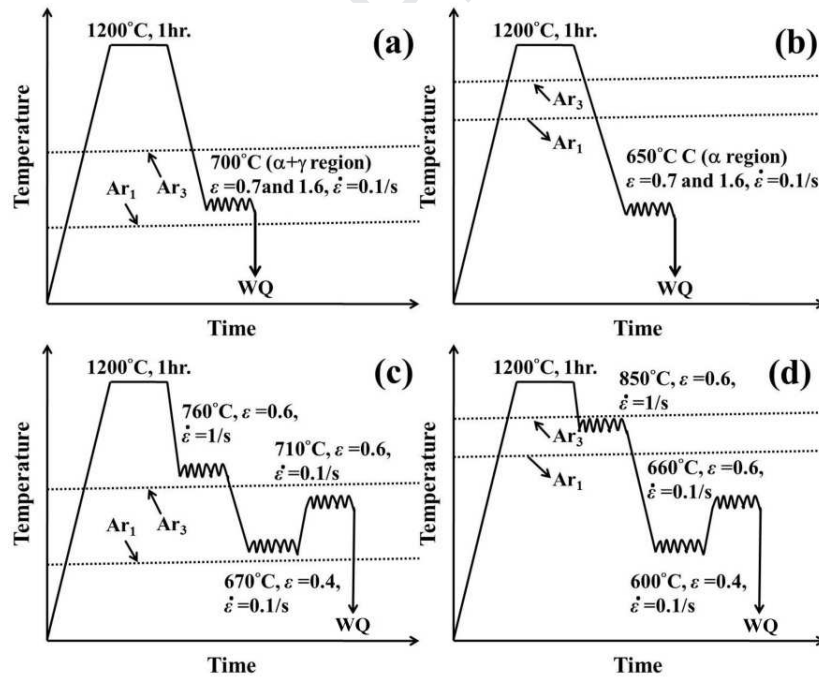

Fig. 1: (a,b) Schematic presentation of the single phase controlled and (c,d) multi-phase controlled rolling schedules for microalloyed and IF steels, respectively.

Secondly, multiphase control 3-steps rolling routes were designed (Figs. 1c and d) for obtaining submicron sized ferrite+martensite in the microalloyed steel and submicron sized ferrite grains in

the IF steel samples. As per the design schedule (as shown schematically in Fig. 1c), the microalloyed steel specimen was first austenitized at 1200°C for 1h. Then the sample was cooled down to 760°C (~Ar_3) at a rate of ~$2°Cs^{-1}$ through normal air cooling. In the first step, the sample was deformed by 45%RA (equivalent strain of 0.6) in single pass at a strain rate of $1s^{-1}$. In the next pass, the same sample was deformed by 30%RA (equivalent strain of 0.4) at 670°C (~Ar_1) at a strain rate of $0.1s^{-1}$ (after cooling the specimen at same rate from 760 to 670°C); and finally in the last pass, the sample was deformed by 45%RA (equivalent strain of 0.6) at 710°C (after reheating the sample to 710°C) a strain rate of $0.1s^{-1}$ followed by WQ at room temperature.

Almost similar kind of TMCP schedule has been designed for the IF steel samples (as shown in Fig. 1d). As per the designed schedule, the austenitized (at 1200°C for 1hr.) IF steel specimen was deformed by 45 (equivalent strain of 0.6), 30 (equivalent strain of 0.4) and 45%RA (equivalent strain of 0.6), respectively, at 850°C (~Ar_3) at a strain rate of $1s^{-1}$, 600°C (~Ar_1) at a strain rate of $0.1s^{-1}$ and at 660°C at a strain rate of $0.1s^{-1}$. After the final hot working step, the sample was WQ at room temperature.

Samples for tensile test were prepared as per ASTM: E8 sub-size standard having a uniform gauge length of 10mm and the test was performed by a Tinius Olsen universal tensile testing machine (Model No: S-Series, H25K-S) having 25kN capacity at a steady strain rate of $2\times10^{-4}s^{-1}$. Fracture toughness of the homogenized, single and multiphase control rolled specimens was investigated by performing 3-point bend tests at room temperature. The 3-point bend tests were executed on same Tinius Olsen machine (25kN capacity) with 3-point bend test fixture, operated at a same strain rate ($2\times10^{-4}s^{-1}$). The specimens for these above mentioned test prepared through the plane parallel to the rolling direction according to the ASTM standard E399-05 (as shown schematically in Fig. 2a and b). Prior to start the 3-point bend test, all the samples were fatigue pre-cracked by EDM wire cutting and maintained a crack length to the width ratio of 0.5 (*a/W*=3.75/7.5). The thickness (*B*) of 3-point bend sample is 3.75mm, while unbroken ligament *b* (*W-a=b*) =3.75mm maintained for all samples (Figs. 2a and b). A set of 3 specimens were tested and averaged for each type of samples.
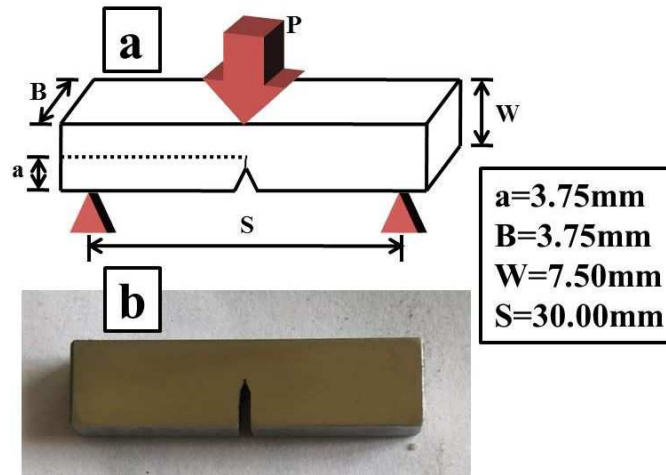
Fig. 2: (a) Schematic presentation of a 3-point bend specimen, (b) photograph of 3-point bend specimen.

Microstructural analysis of control rolled samples was investigated through optical microscopy, transmission electron microscopy (TEM), scanning electron microscopy (SEM) and EBSD studies. Leica DMI5000M microscope was used for optical microscopy. Samples prepared for optical microscopy was subsequently polished using different emery papers and cloth followed by chemical etching using 2% Nital solution. The quantitative measurement of low and high angle grain boundaries present and their distribution in deformed state were examined through EBSD analysis. All the selected samples for the EBSD analysis were first cloth polished using alumina powder and then using colloidal solution of silica+methanol. Finally, the specimens were electropolished for 50s using an electrolyte of 80% methanol+20% perchloric acid at -20°C at an applied voltage of 21V. The EBSD analysis was carried out using HKL channel-5 system software attached with SEM (Model No: ZEISS, 51-ADD0048). The surface which is parallel to the compression axis of the deformed specimen was analyzed. The step size (0.1μm) was kept low to track the misorientation and the frame size was about 150mm×150mm.TEM analysis was performed using FEI Technai 20 G2S-Twin electron microscope, operated at 200 kV. The specimen for TEM study were first thinned down up to 0.08μm through mechanical polishing using SiC abrasive papers starting from 800 to 2000 grit size sequentially. After that 3 mm disk specimens were punched out using a Gatan disk cutter from this thin foil (<80μm). In final stage, twin jet electro-polishing was carried out using a solution of 10% perchloric acid+90% methanol at -20°C using 40V potential difference. Failure analysis of all the fractured surfaces after 3-point bend test were studied under SEM.

3. Results and discussion

3.1 Microstructural characterization

The optical micrographs of the homogenized annealed (H-AN) microalloyed and IF steel specimens are shown in Figs. 3a and b, respectively. The microstructure of the microalloyed H-AN specimen exhibits equiaxed pro-eutectoid ferrite and lamellar pearlite (alternate plates of ferrite and cementite) with an average grain size of ~56µm. On the other hand, the IF H-AN sample exhibits larger size equiaxed pro-eutectoid ferrite grains (average grain size was assessed to be 110µm). Pearlite is not found to be present in the microstructure of IF steel due to extremely low C content (0.0026%).

The optical micrograph is shown in Fig. 4a for the single phase controlled (at α+γ region) 50% reduction in area (RA) microalloyed steel sample deformed at a strain rate 0.1s^{-1} followed by WQ. The micrograph is consisted two types of ferrite grains (fine subgrains with average grain size 5µm and larger size grains with average grain size 22µm) and martensite.
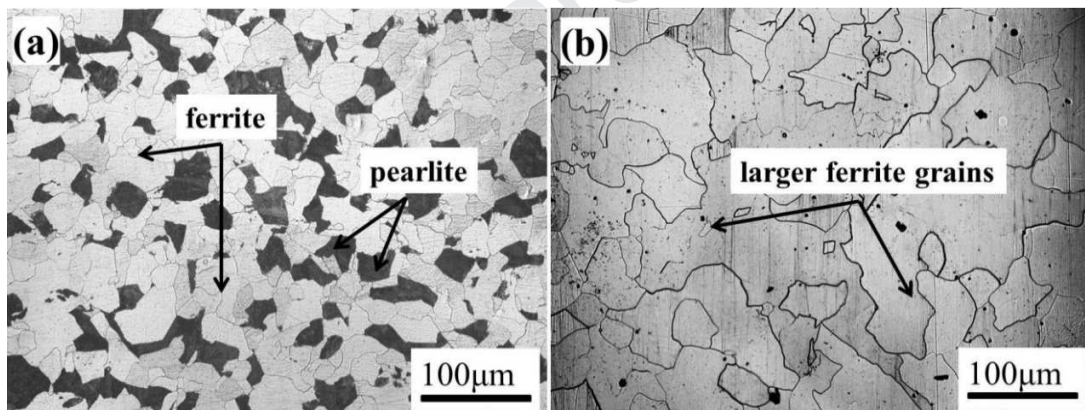

Fig. 3: Optical microstructure of homogenized annealed (a) microalloyed and (b) IF steel specimen.

Fine subgrain formation occurred mainly through deformation induced ferrite transformation (DIFT) mechanism. After WQ the remaining austenite plausibly transformed into martensite and the deformed ferrites retained their morphology without any subsequence growth.
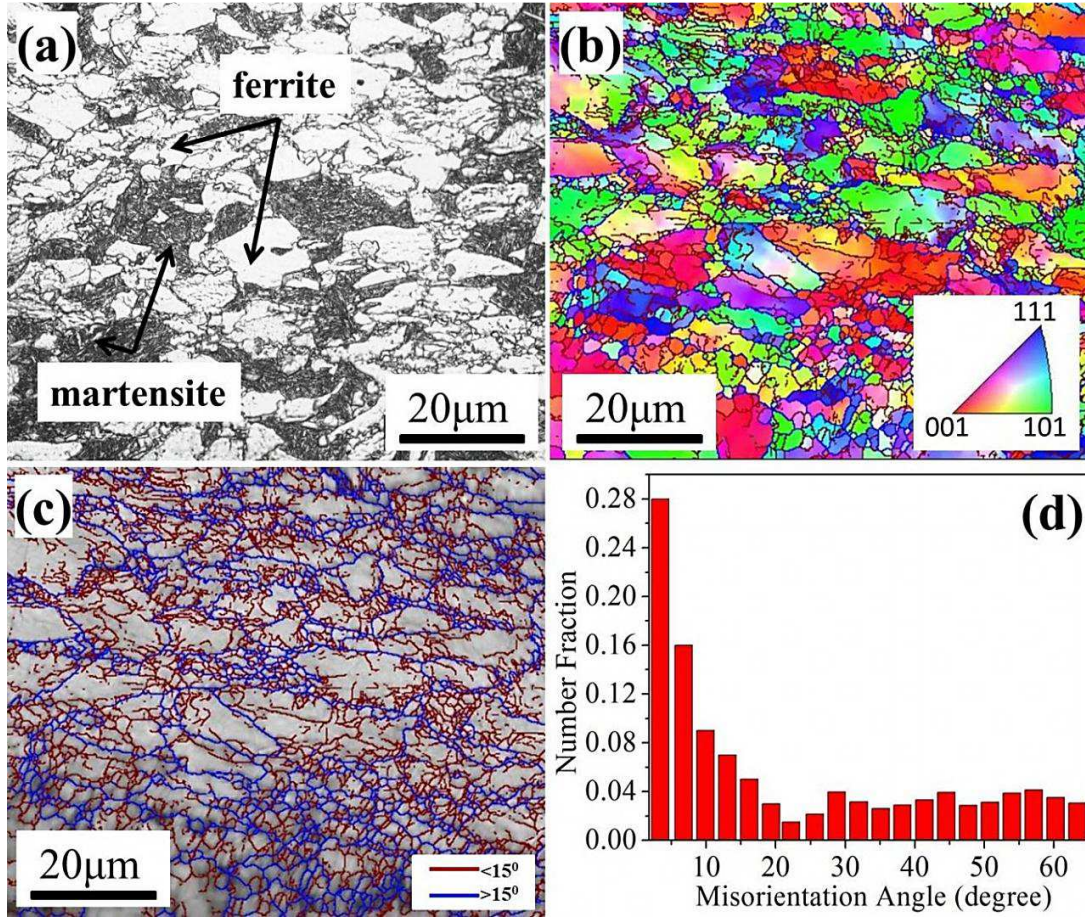
Fig. 4: (a) Optical microstructure, (b) EBSD inverse pole figure map, (c) grain boundary map of α+γ region control rolled (50%RA) microalloyed steel specimen, (d) misorientation profile of the corresponding microstructure.

Figs. 4b and c represents the EBSD inverse pole figure and grain boundary maps, respectively, of this specimen. Fine ferrite subgrains are found to embed within the larger size elongated ferrite and martensite regions. It can clearly be identified from the EBSD grain boundary map (Fig. 4c) that new the grains formed on the grain boundaries of the preexisting grains. In the grain boundary map (Fig. 4c), the grain boundaries are separated by two different colors based on the misorientation angle. Blue lines indicate the misorientation angle >15° i.e. high angle grain boundaries (HAGBs); whereas, red lines refer to misorientation angles <15°, i.e. low angle grain boundaries (LAGBs) or sub-grain boundaries (SGBs). It can clearly be observed that several LAGBs are introduced within the elongated ferrite grains, which indicate that the original grains were partitioned by formation of LAGBs through dynamic transformation. Fig. 4d represents the misorientation profile of corresponding microstructure. Misorientation angle distribution of the ferrite grain boundaries exhibited (Fig. 4c) that numerous LAGBs were introduced within the

8

ferrite grains bounded by HAGBs. Moreover, certain fractions of fine ferrite grain bounded by HAGBs are existed within the large ferrite grains.

Furthermore, it can be observed that with further increasing the %RA (i.e. after 80%RA) the fraction of the fine ferrite grains increased and developed a bimodal ferrite grain structure (1-3μm+10-12μm) along with martensite (av. size ~15μm) (Figs. 5a and b). This is attributed to the formation of more substructures within the ferrite grains with increasing the amount of deformation. When the amount of deformation energy attained equivalent to the recrystallization activation energy, fine equiaxed recrystallization ferrite grains are developed. It can also be seen from Figs. 5c and d that the fraction of LAGBs relatively decreased and HAGBs fraction increased after 80% RA as compared to that of the 50% rolled specimen.

Generally, in case of high stacking fault energy materials, dynamic recovery (DRV) is contemplated as the only governing mechanism during deformation. However, the dynamic recrystallization (DRX) of ferrite was noticed to occur in low C steel deformed in α+γ phase region [17,18]. Recently, Sakai et al. [9] and Zhao et al. [11] reported that the continuous dynamic recrystallization (CDRX) of ferrite could occur in ferrite during deformation [9,11]. During CDRX process the misorientation between subgrain boundaries of ferrite constantly increases with raising the amount of strain until the subgrain boundaries change to HAGBs.
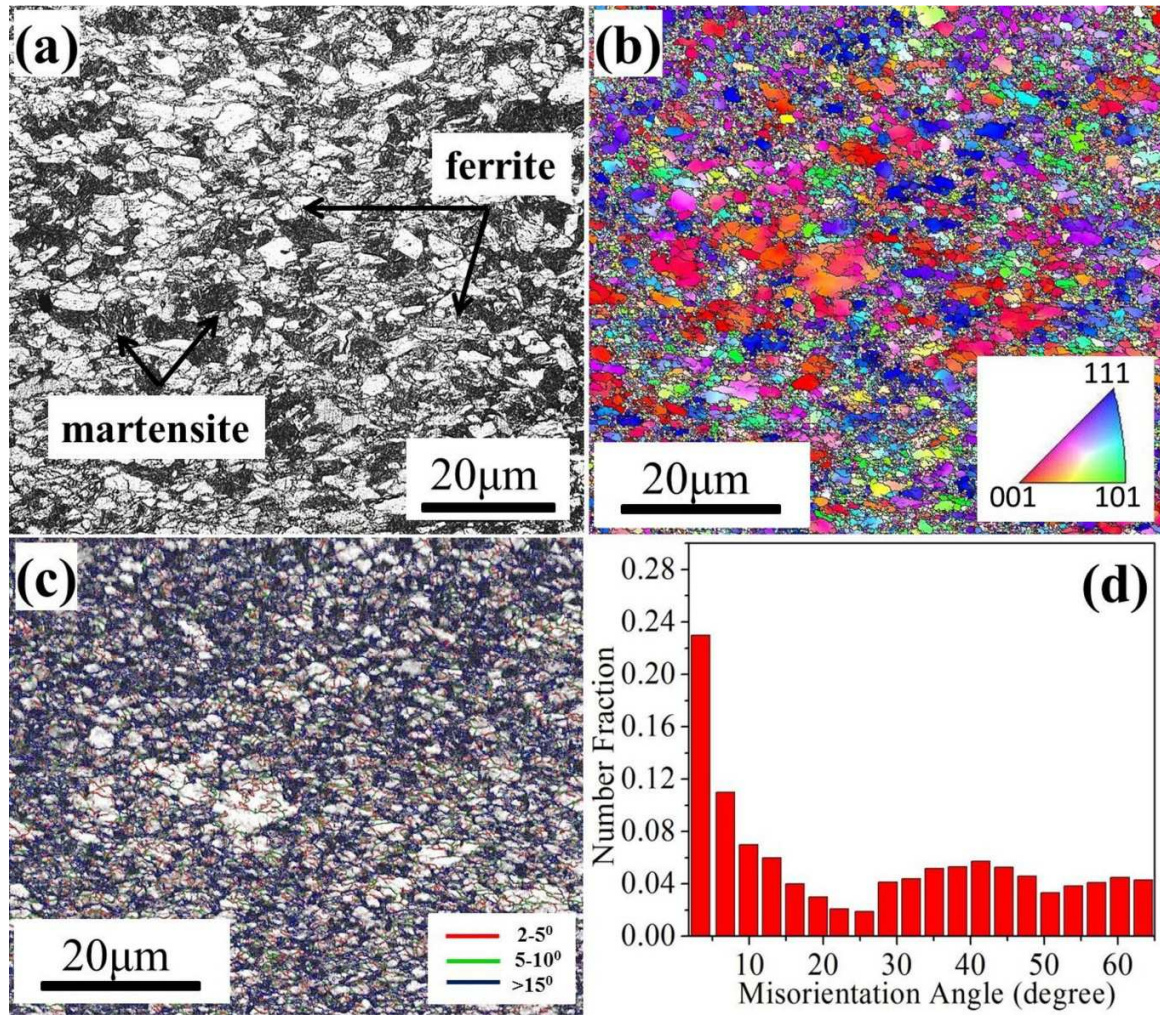
Fig. 5: (a) Optical microstructure, (b) EBSD inverse pole figure map, (c) grain boundary map of α+γ region control rolled (80% RA) microalloyed steel specimen, (d) misorientation profile of the corresponding microstructure.

The EBSD grain boundary map (Fig. 4c) presented that few fraction of equiaxed fine ferrite grains formed in the deformed ferrite grains after 50% deformation. Moreover, it can be seen from Fig. 5c that the fraction of equiaxed fine ferrite grains increased with increase in the amount of deformation (80%RA). The misorientation between subgrain boundaries of ferrite also increases (Fig. 5d). Thus, high amount of deformation (80% RA) in the α+γ region (e.g., 700°C) resulted in the CDRX of the deformed ferrite.

On the other hand, in the IF steel sample 50% rolled in pure ferritic region at ~650°C, major fraction of the ferrite grains is found to elongate in the rolling direction. Moreover, formation of deformation bands along with a few fractions of recrystallized grains within the deformed bands can be seen from the micrograph of the specimen (Fig. 6a). The microstructure of the IF steel

sample revealed two types of ferrite grains: ~80% of the elongated grains and ~20% of the subgrains with an average size of ~1-3µm (Fig. 6a). Moreover, formation of relatively large fraction of subgrains along with the micro-shear bands can be seen after 80% rolling of the IF steel (Fig. 6b).
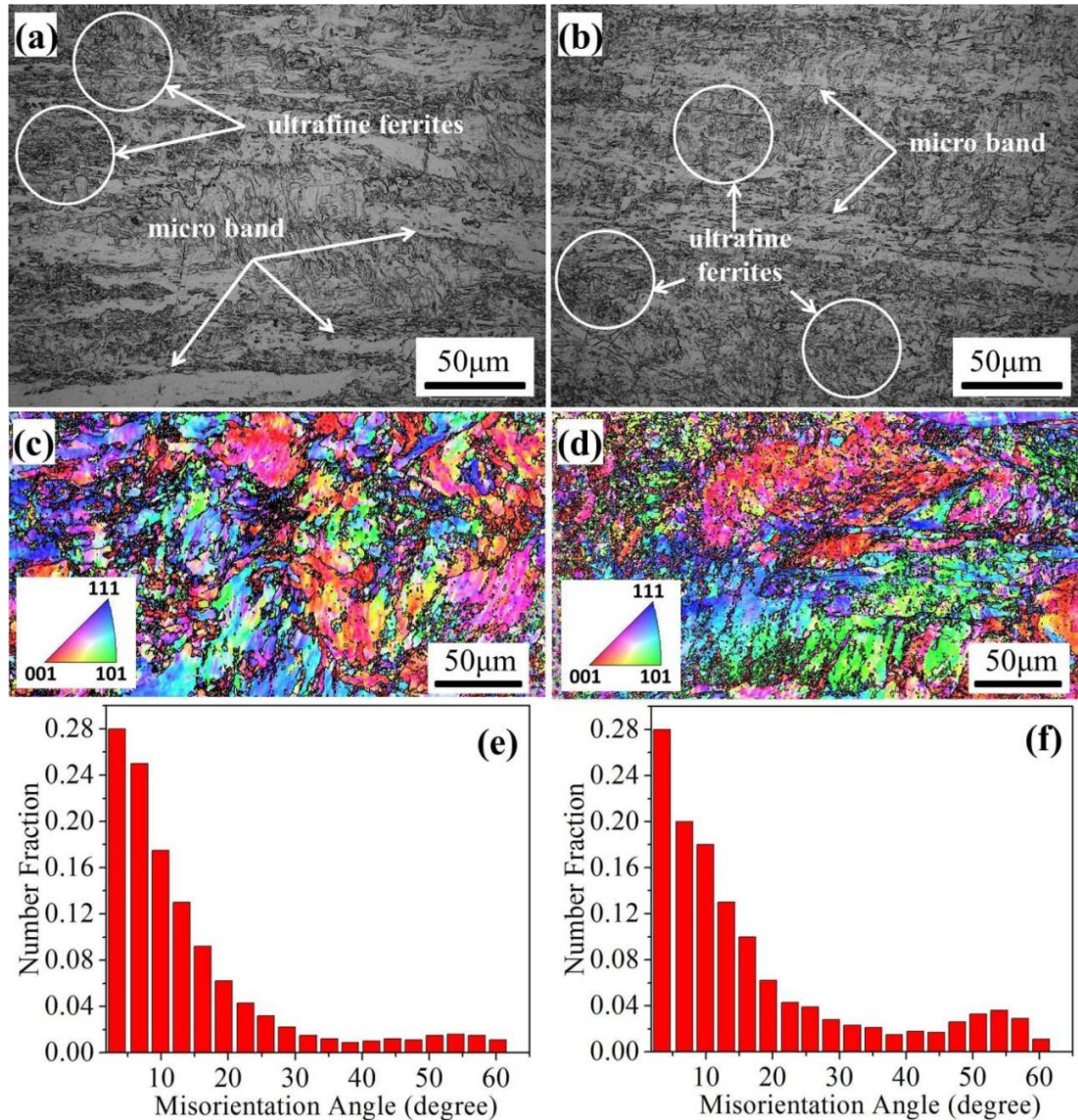
Fig. 6: (a,b) Optical microstructures, (c,d) EBSD inverse pole figure map of α region control rolled 50 and 80%RA IF steel specimens, respectively, (e,f) misorientation profile of corresponding specimens, respectively.

Figs. 6c and d represents the EBSD inverse pole figure map of α-region control rolled 50and 80%RA IF steel specimens, respectively. Regions of fine grained ferrite grains embedded within the larger size ferrite are clearly manifest from both the EBSD images (Figs. 6c,d). In case of

80% rolled specimen (Fig. 6d), a large number of ultra-fine ferrite grains can be seen as compared to than that of 50% rolled specimen (Fig. 6c). In both cases the EBSD images (Figs. 6c,d) clearly reveal the appearance of various new ferrite grains along the grain boundaries of the pre-existing larger ferrite grains. The grain boundary misorientation distribution map of 50% rolled specimen (Fig. 6e) showed that several LAGBs were generated in individual ferrite grains along with relatively low fraction of HAGBs. But after 80%RA (Fig. 6f), more HAGBs were introduced into the ferrite grains, and the size of the subgrains and the fraction of LAGBs further decreased (Figs. 6f) which indicated the occurrence of DRX.

The coarse-grained ferrite becomes strain hardened and the density of dislocation gradually increases through repeated deformation. Consequently, a large number of subgrains or dislocation cells are originated within the deformed ferrite grains and at the ferrite grain boundaries. These subgrains finally recovered and recrystallized to generate new equiaxed strain-free grains [8,19,20]. Moreover, it is well known that decreasing the deformation temperature can endorse dynamic strain induced ferritic transformation (DIFT) phenomena [20] and subsequently, reduces the ferrite grain size. Furthermore, formation of micro-shear bands during deformation generated new dislocations, and with increase in the deformation accumulation of dislocations gradually increased and reorganized between them [21]. It also raises the grain boundary misorientation through transformation of LAGBs to HAGBs and finally leads to the creation of ultrafine ferrite grains [21].

Overall, it can be observed that the DIFT and DRX are two important mechanisms to develop fine ferrite grains during the single phase control multi-pass rolling of both the IF and microalloyed steels. But unfortunately, through conventional DRX/DIFT mechanism the ferrite grain refinement has reached the limitation within the range of 2-4µm [7,10] which is also observed in the present study (Figs. 5b and 6d). Thus, advanced 3-steps multiphase control thermomechanical processing schedule has been designed with an aim to achieve ultrafine ferrite grains, i.e., <1µm. Details rolling schedules are shown in experimental details section (Figs. 1c and d). It can be observed from Fig. 7a that the ultrafine ferrite (UFF) grains along with fine martensite are obtained after 3-steps multi-phase control rolling of the microalloyed steel as per designed schedule as shown in Fig. 1c. The average grain size of UFF is estimated to be ~0.69µm (as shown in the EBSD image, Fig. 8a and TEM bright field image, Fig. 10a). On the other hand, UFF structure is estimated to be ~0.83µm (as shown in the EBSD image, Fig. 9a and

TEM bright field image, Fig. 10b) after 3-steps multiphase control rolling of the IF steel as per designed schedule.
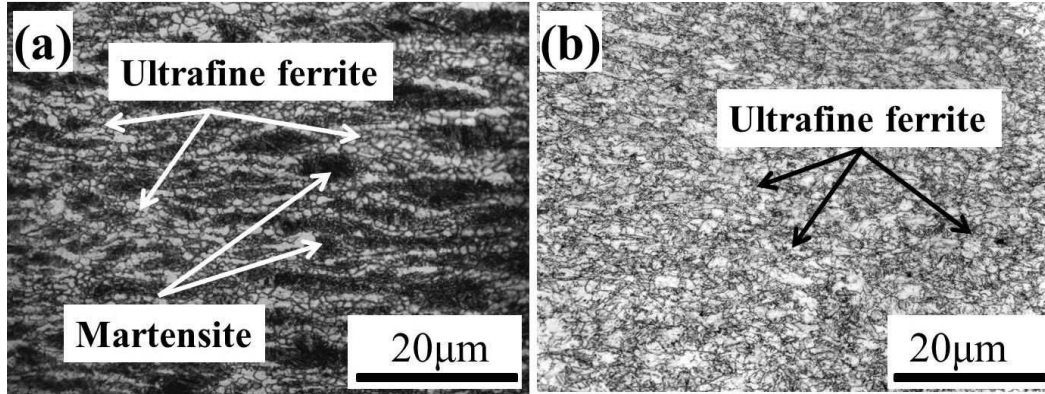

Fig. 7: Optical microstructures of 3-steps multi-phase control rolled (a) microalloyed and (b) IF steel as per designed schedule, respectively.
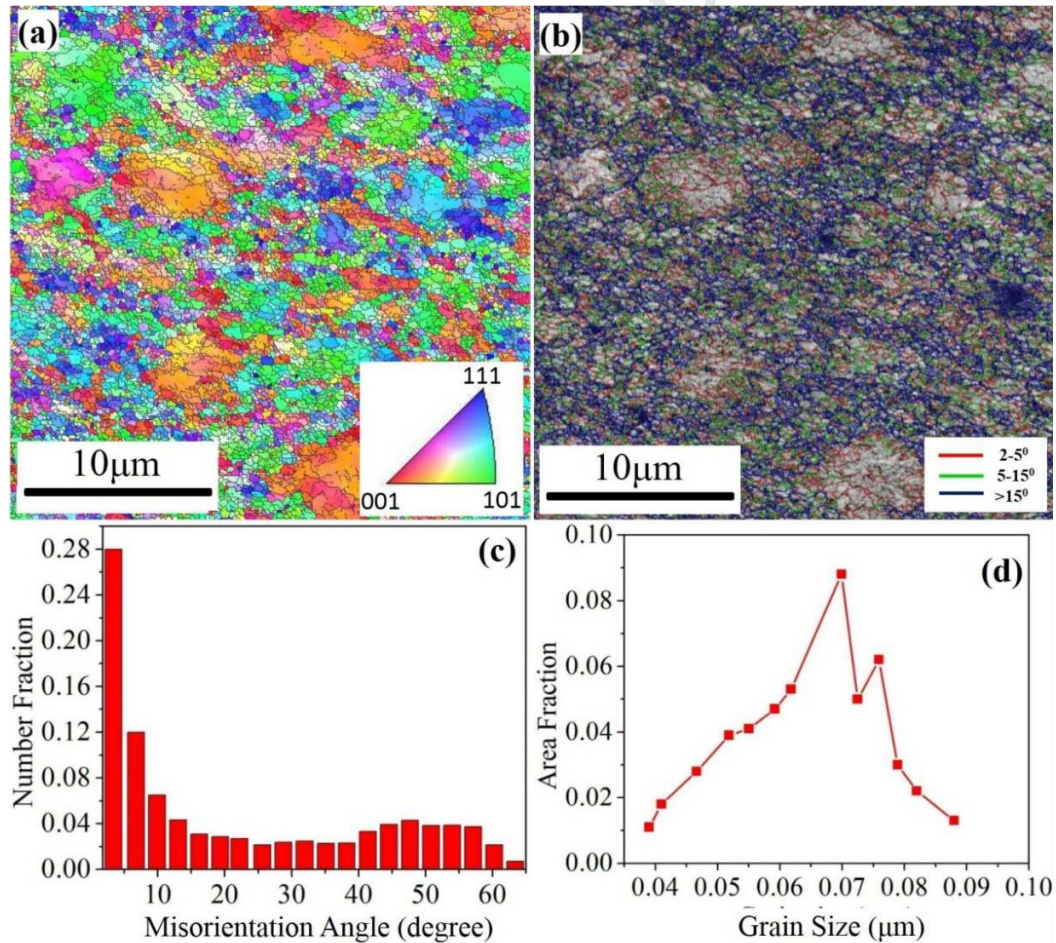

Fig. 8: (a) EBSD inverse pole figure and (b) grain boundary maps of 3-steps multi-phase control rolled microalloyed steel as per designed schedule; (c,d) Misorientation profile and grain size distribution of corresponding specimen, respectively.

Figs. 8a,b and 9a,b represent the EBSD inverse pole figure and grain boundary map, respectively, for the 3-steps multi-phase control rolled microalloyed and IF steels as per designed rolling schedules. It can be observed from Figs. 8b and 9b that the large fractions of ferrite subgrains are present within the coarse ferrite grains. Thus, LAGBs are observed within the coarse ferrite grains, indicating that a deformed structure is introduced. Moreover, equiaxed ultrafine ferrite (UFF) grains surrounded by HAGBs start to form along the grain boundaries of coarse ferrite.

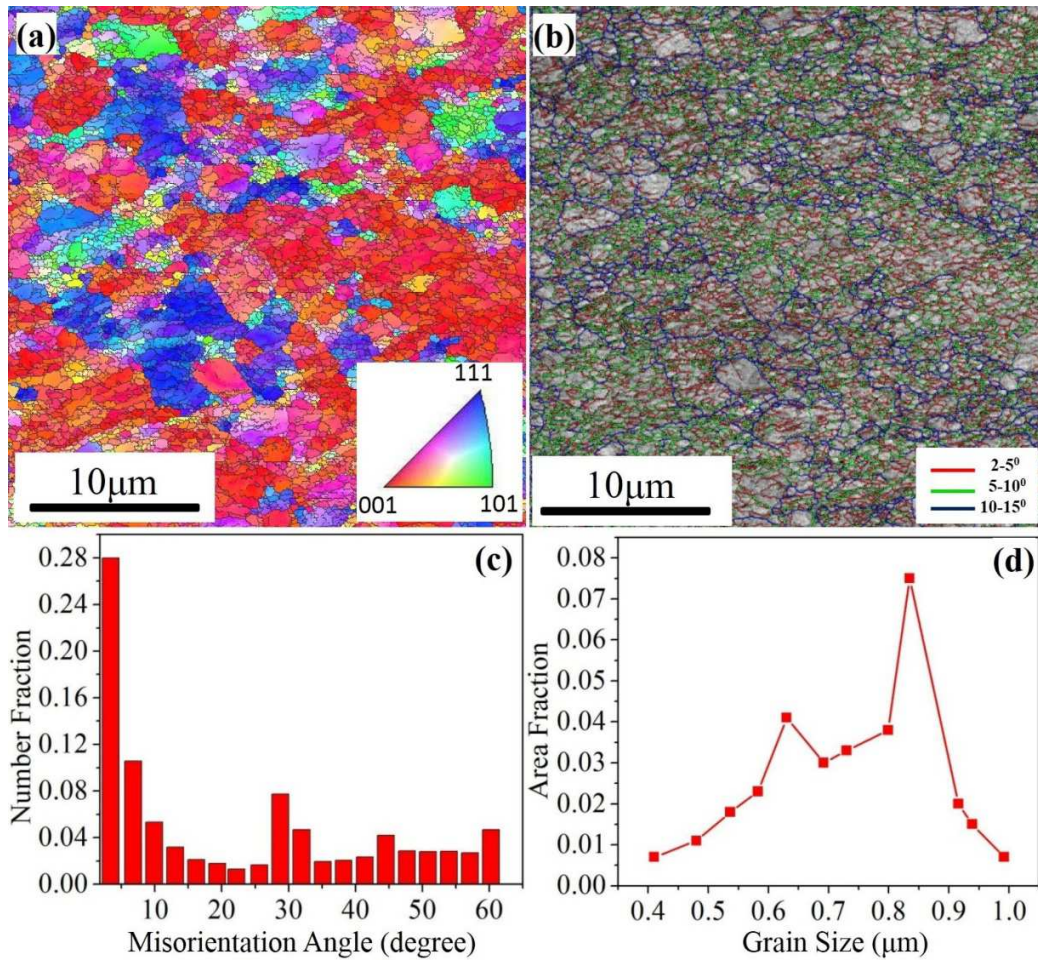Fig. 9: (a) EBSD inverse pole figure and (b) grain boundary maps of 3-steps multi-phase control rolled IF steel as per designed schedule; (c,d) Misorientation profile and grain size distribution of corresponding specimen, respectively.

The misorientation profile and grain size distribution profile of the corresponding specimens are shown in Figs. 8c,d and 9c,d respectively. Average grain sizes (0.69µm and 0.83µm,

respectively, for microalloyed and IF steel samples) of the corresponding specimens are estimated from the grain size distribution profile as shown in Figs. 8d and 9d.
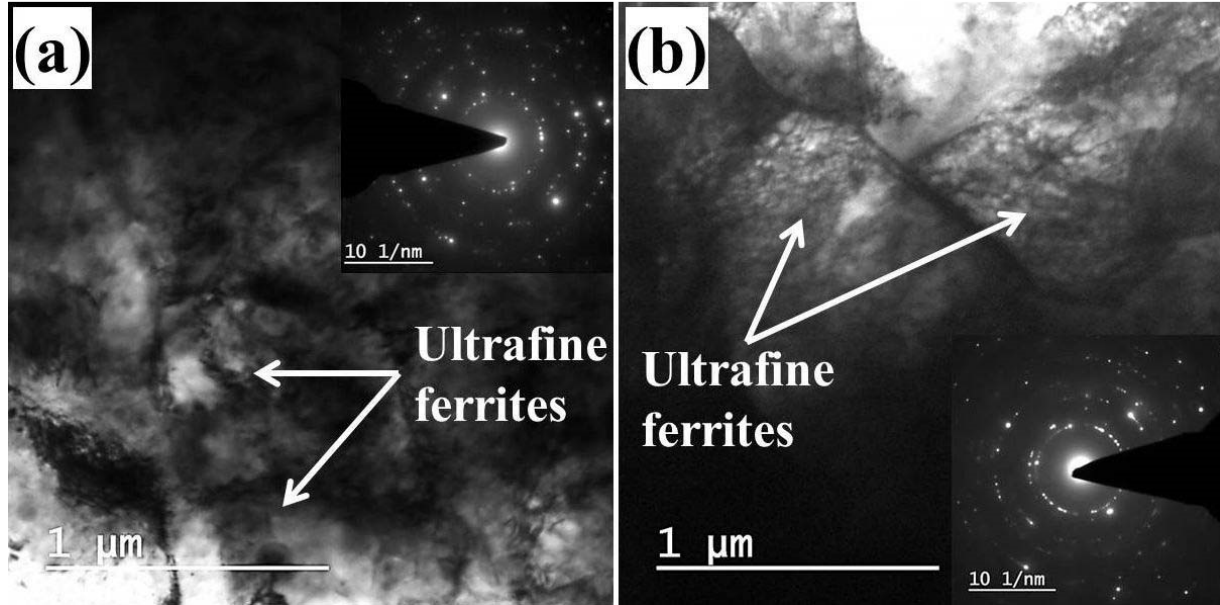

Fig. 10: TEM bright field image of 3-steps multi-phase control rolled (a) microalloyed and (b) IF steel as per innovative designed schedule.

The mechanism of ferrite grain refinement can be interpreted as follows: when deformation is carried out at around $\sim A_{r3}$ region, fine ferrite is dynamically transformed from austenite grains. Further deformation at around $\sim A_{r1}$ region, the ferrite grains are refined further through subgrain formation. After 3rd pass of the rolling (Fig. 1c) at relatively higher temperature (compared to 2nd pass), the ferrite grains are further refined through dynamic recrystallization of the transformed ferrite grains and developed an equiaxed UFF grain structure. The first pass deformation was selected (equivalent strain=0.6) at 760°C ($\sim A_{r3}$ temperature region) to accelerate the strain induced ferrite transformation. The lattice defects were introduced within the austenite grains through deformation at 760°C ($\sim A_{r3}$). These defects could provide more sites of nucleation for the ferrite transformation and thereby accelerating the DIFT. Subsequently, the grain size of the deformation induce transformed ferrite was found to be very fine due to the enhanced nucleation. It is believed that the reduction in the grain size can decrease the critical strain required for initiating DRX and thereafter accelerates the kinetics of DRX [22-24]. It should be further highlighted that the total deformation is mostly performed within the $\alpha+\gamma$ region. Ferrite phase is softer than the austenite at high temperature in $\alpha+\gamma$ region [17,25] so that the introduced plastic

strain would concentrate more on the ferrite grains, which could also boost the DRX of ferrite grains. Similarly, UFF structure is obtained after 3-steps multiphase control rolling of the IF steel as per designed schedule as shown in Fig. 1d. In this case, average grain size of the UFF is estimated to be ~0.83µm (as shown in the EBSD image, Fig. 9a and TEM bright field image, Fig. 10b). The mechanism of formation of the UFF could be explained in the same direction, i.e., DRX of deformation induce transformed ferrite, as described above for the microalloyed steel samples.

3.2 Mechanical Properties

The engineering stress *vs.* strain plots of the thermomechanical control rolled (TMCRed) microalloyed and IF steel specimens are presented in Figs. 11a and b, respectively and summarized in Table 2 for better convenience. The yield strength (YS) of the homogenized annealed (H-AN) specimen is estimated to be ~251 and 141MPa along with a good amount of tensile ductility of 33 and 46%, respectively, for microalloyed and IF steel samples. The high ductility is endorsed to the formation of large size ferrite and lamellar pearlite with an average grain size of ~56µm in case of microalloyed steel and comparatively larger size ferrite grains (~110µm) in case of IF steel specimens. The YS and ultimate tensile strength (UTS) of the α+γ phase control rolled (80%RA) microalloyed steel samples are found to enhance to 811 and 937MPa, respectively. It can be seen that the improved YS (811MPa) of the α+γ phase control rolled sample is 3 times higher than that of the homogenized annealed specimen (251MPa). It can also be observed from Fig. 11a that the YS and UTS of the selected phase control rolled specimens increased significantly having reasonably high amount of retained ductility. The tensile ductility of the H-AN sample was found to be ~38% and the corresponding microstructure showed an average grain size of ~56µm (Fig. 3a). The specimen deformed at α+γ phase region exhibited a tensile ductility of ~19%. It has been already described earlier that the microstructure of the specimens deformed at the α+γ phase region consisted of 3 different types of grain structure (Fig. 5a); large size ferrite (10-12µm), fine ferrite grains (1-3µm size) and martensite structure (~15µm). It was observed that the YS of the specimens are significantly enhanced without much sacrificing the ductility when deformed in α+γ phase region followed by water quench. This is attributed to the extensive grain refinement attained through CDRX mechanism. It is well established that the grain refinement is a very effective way to improve the

16

strength of metallic materials without much losing their %elongation [26]. Hence, development of fine ferrite grains is responsible to enhance the YS, whereas relatively larger size ferrite grains retaining its ductility.

Table 2: The Mechanical properties of the Homogenized annealed (H-AN) and TMCRed microalloyed and IF steel specimens.

Rolling conditions		YS (MPa)	UTS (MPa)	% Elongation
Microalloyed steel	H-AN sample	251±4	440±5	33±1.7
	TMCRed at 700°C sample	811±8	937±9	19±1
	3-steps control TMCRed sample	923±4	1101±3	13.6±1.5
IF steel	H-AN sample	141±3	256±5	46±1.7
	TMCRed at 650°C sample	421±5	479±3	27±2
	3-steps control TMCRed sample	623±4	651±3	19±1.5

Similarly, the IF steel specimen deformed (80%RA) in pure α region exhibits the maximum enhancement in the YS (421MPa) and UTS (479MPa). It is to be noted that the improved YS (421MPa) is about 3 times higher than that of the H-AN specimen (141MPa). Furthermore, it can be found (Fig. 11b) that the YS and UTS of the pure ferritic phase control rolled specimen enhance with a slight loss of ductility (27%) as compared to that of the H-AN specimen (46%). It is attributed to the development of a dual size grain structure, where fine ferrite grains (Fig. 6d) are responsible for the improvement of YS and relatively larger size ferrite grains retain the ductility. Godha et al. [20] also observed the formation of dual size ferrite grains in plain C-Mn steel deformed in the inter-critical regime (at ~730°C) which yielded a good combination of YS and ductility.
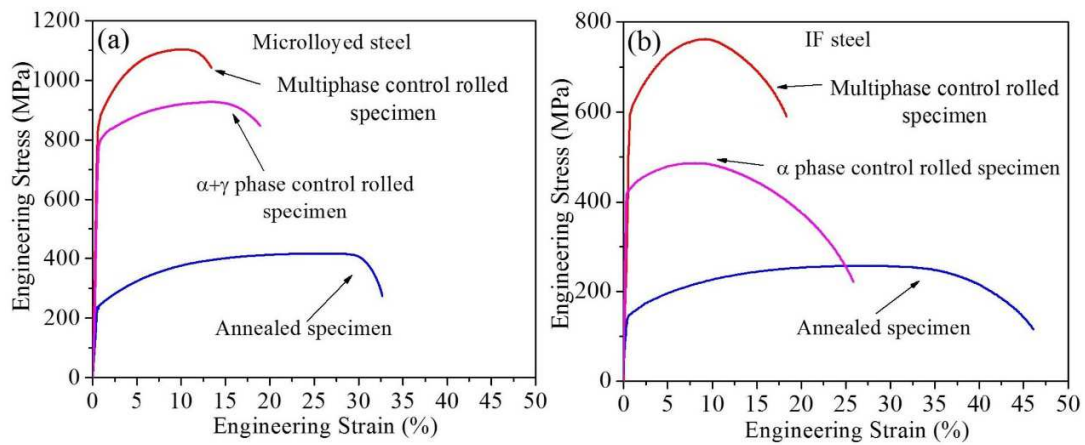

Fig. 11: Tensile stress-strain curves of TMCRed (a) microalloyed and (b) IF steel specimens.

Furthermore, it can be noted that the multiphase control rolled sample as per the designed schedule (Fig. 1c) shows a significant improvement of the YS (923MPa) corresponding to a ultrafine grain size of 0.69μm (Figs. 8a and d) for the microalloyed steel (Fig. 11a); whereas, the IF steel sample shows an improved YS of 623MPa (Fig. 11b) corresponding to a grain size of 0.83μm (Figs. 9a and d). As per the reported literature, the YS in the present study are much superior for the ultrafine grained microalloyed and IF steel specimens achieved through the innovative control rolling schedules. The prime reason of such improvement is the refinement of the ferrite grains to sub-micron level (<1μm). It should be emphasized that in the present processing route, the equivalent strain given per pass is relatively smaller than those previously reported literature [10,27] though the total imposed strain is same (i.e. 80%RA as in the present study). Furthermore, it is known that ultrafine ferrite grains usually show limited amount of ductility due to excessive strain hardening [28]. In such context, it is highly encouraging that the present ultrafine ferrite (UFF) structure (developed through combination of DIFT and DRX mechanisms) maintains a significant amount of tensile ductility, i.e. 13.5 and 19%, respectively, for the microalloyed and IF steels as shown in Figs. 11a,b and Table 2. This is mainly due to the formation of dynamically recrystallized UFF equiaxed microstructure. It is well known that free/mobile dislocations always exist in the dynamically recrystallized microstructure, which could accommodate more amount of plastic deformation during tensile deformation. In the ultrafine microstructure with submicron size grains, the existence of mobile dislocations may contribute to an improved ductility in the metallic materials [29], which is an interesting phenomenon and requires further investigation.

3.3 Investigation of fracture toughness of ultrafine grained steels

Generally, the formability as well as ductility of the UFG metallic materials is found to deteriorate due to their reduced strain hardening response. Analysis of fracture toughness could provide more detail information about the deformation characteristics and fracture activities of such UFG materials [13]. Evaluate the fracture toughness of the UFG materials is challenging because of size limitation of the processed metals/alloys. Hence, hardly any data is available about the valid K_{IC} (plane strain fracture toughness) of the UFG steels owing to the limited specimen dimensions, especially the thickness, obtained through advanced thermomechanical control rolling. Recently, some researchers [14-16] tried to evaluate the fracture toughness values

by 3-point bend tests of nonferrous UFG materials and reported that the grain size refinement has significant effect on the improvement of conditional fracture toughness. Recently, the microalloyed and IF steels have been extended in several structural applications (ship building, automotive, line pipe etc.), where knowledge of fracture toughness is extremely vital. Thus, though the UFG steels in the present study show exceptional improvement of mechanical properties, investigation of fracture toughness is extremely important for any structural applications. Some samples (which showed good combination of YS and %El.) were selected to study the fracture toughness values to enlighten the deformation characteristics of the UFG steels. Due to limitation of the sample thickness, investigation of fracture toughness of the UFG steels has been performed through computing conditional fracture toughness (K_Q), equivalent energy fracture toughness (K_{ee}) and J-integral (crack initiation energy) from 3-point bend test data and correlated with other mechanical properties. The specimens for 3-point bend test were prepared as per the ASTM standard E399-05. Details of sample preparation have been discussed in materials and experimental procedure section (section 2).

The requirement of minimum thickness for accomplishing plane strain situations i.e. for valid K_{IC} calculation could be estimated using Eq. 1 [30].

$$B = 2.5 \left(K_{IC} \big/ \sigma_{YS} \right)^2 \tag{1}$$

where, σ_{YS} is the yield strength (0.2% offset). In order to evaluate linear elastic plane strain fracture toughness, the maximum recorded load, P_Q, could be estimated from the load *vs.* extension curve as presented in Fig. 12a. The value of P_Q could be substituted in Eq. 2 for evaluating the apparent fracture toughness value, K_Q [30].

$$K_Q = \frac{P_Q}{B} \frac{S}{W^{3/2}} \left[2.9 \left(\frac{a}{W} \right)^{\frac{1}{2}} - 4.6 \left(\frac{a}{W} \right)^{\frac{3}{2}} + 21.8 \left(\frac{a}{W} \right)^{\frac{5}{2}} - 37.6 \left(\frac{a}{W} \right)^{\frac{7}{2}} + 38.7 \left(\frac{a}{W} \right)^{\frac{9}{2}} \right] \tag{2}$$

where, a is the length of the crack.

Furthermore, the applicability of the test is justified using Eq. 3 as follows:

19

$$B = 2.5 \left({K_Q}/{\sigma_{\text{YS}}} \right)^2 \qquad (3)$$

K_Q can be recognized as plain strain fracture toughness (K_{IC}), only if the value of B is less than both the crack length and thickness of the sample [30] and then Eq. 1 is valid; else K_Q is considered as conditional fracture toughness.

The load-extension curves for the thermomechanically control rolled microalloyed and IF steel samples are presented in Figs. 12b and c. It was observed from the Fig. 12a that the maximum load (P_Q), at which pre-existing crack grows to a critical size, comes out to be 2478N for the $\alpha+\gamma$ phase control rolled microalloyed steel sample. This limiting load is switched in Eq. 2 for determining the apparent fracture toughness values, K_Q. On replacing the values of P_Q, W, B and a in Eq. 2, the value of K_Q is calculated to be 46.8MPa$\sqrt{\text{m}}$ for the $\alpha+\gamma$ phase control rolled microalloyed steel sample.
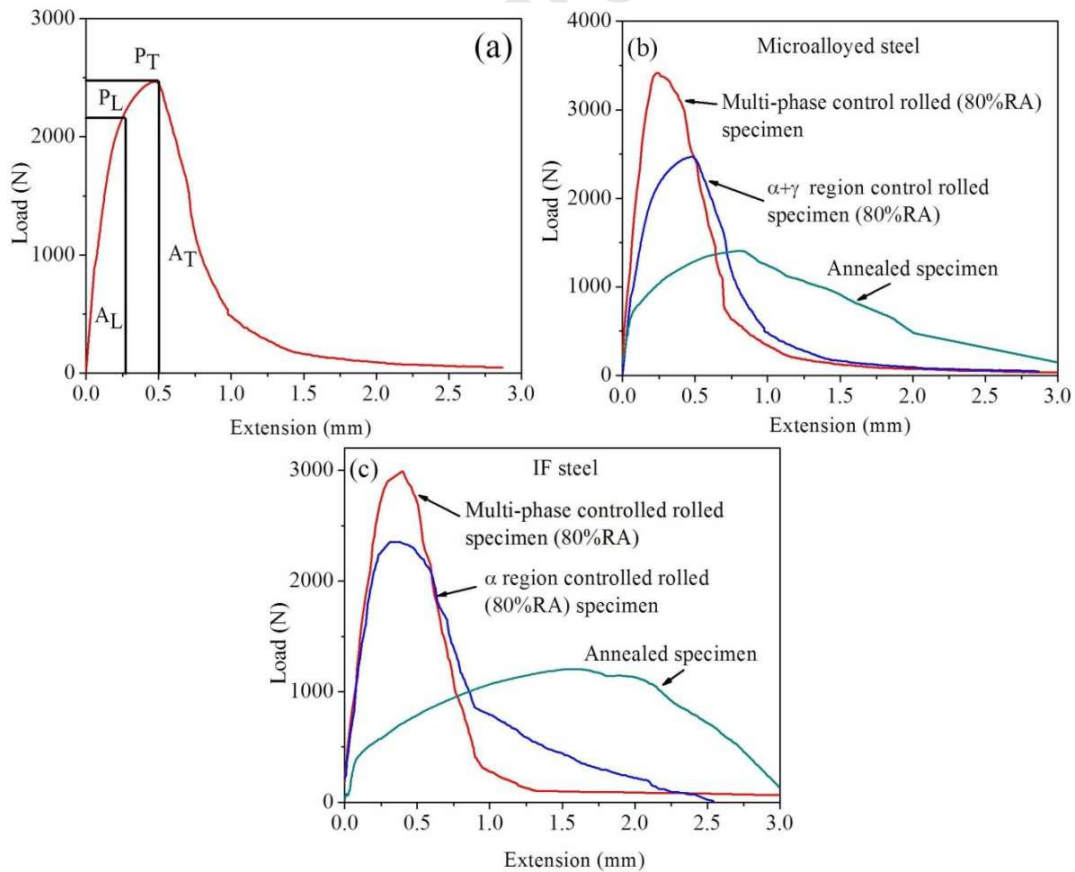

Fig. 12: (a) Representative load *vs*. extension plot for the $\alpha+\gamma$ phase control microalloyed steel sample to calculate the equivalent load, P_E, used to evaluate equivalent fracture toughness, K_{ee}, (b,c) Load *vs*.

extension curves of microalloyed and IF steel specimens rolled in different processing conditions, respectively.

The same method was monitored to evaluate conditional values of fracture toughness, K_Q, for the other selected specimens and the values are summarized in Table 3. In order to verify the applicability of the 3-point bend test, the experimentally obtained value of YS and K_Q, were substituted in Eq. 3 and it was found that the values of B for all the specimens are greater than the crack length and actual thickness of the corresponding specimen. As the value of K_Q obtained from 3 point bend test using linear elastic fracture mechanics (LEFM) could not fulfill the validity requirement. Thus in the present study we have considered another approach to determine the equivalent energy fracture toughness (K_{ee}) as per ASTM standard E 992 using the following equations (Eq. 4 and 5) [15,31]. In this method, the equivalent load, P_E has to be evaluated instead of provisional load, P_Q as per ASTM standard E 992 [32]. In this method, area A_L under load *vs.* extension curve up to linear part P_L needs to be determined first; then, the area A_T up to maximum load is being calculated. Furthermore, J-integral values also have been determined to enlighten the comparative improvement of the fracture toughness and correlate with the other mechanical properties as well as microstructural features [32].

$$K_{ee} = \frac{P_E}{B} \frac{S}{W^{3/2}} \left[3 \left(\frac{a}{W}\right)^{\frac{1}{2}} \frac{\left[1.99 - \frac{a}{W}\left(1 - \frac{a}{W}\left(2.15 - 3.93\frac{a}{W} + 2.7\frac{a^2}{W^2}\right)\right)\right]}{2\left(1 + 2\frac{a}{W}\right)\left(1 - \frac{a}{W}\right)^{3/2}} \right] \tag{4}$$

$$P_E = P_L \sqrt{\frac{A_T}{A_L}} \tag{5}$$

Fig. 12a shows the representative load *vs.* extension plot for the α+γ phase control rolled microalloyed steel sample to calculate the equivalent load, P_E, used to assess equivalent fracture toughness, K_{ee} (Fig. 12a). In this case, A_T = 1213N-mm, P_T = 2478N, A_L = 813N-mm, P_L = 2161N. The equivalent load, P_E is estimated to be 2639.6N. This value of P_E is substituted in Eq. 4 and the K_{ee} for the multiphase control rolled microalloyed steel sample was calculated to be 68.9MPa$\sqrt{m}$. In similar way, K_{ee} has been evaluated for all the other specimens and represented in Table 3 along with values of K_Q and J-integral of the corresponding specimen.

It should be noted that fracture toughness of structural materials strongly depends on initiation and propagation of crack. There are 2 approaches commonly used to evaluate fracture toughness i.e. (i) linear elastic fracture mechanics (LEFM) and (ii) elastic plastic fracture mechanics

(EPFM). LEFM approach is used to examine crack initiation (K_Q), while EPFM approach interprets crack propagation (J-integral). Hence, fracture toughness of UFG materials could be enhanced through hindered crack initiation. In this work, conditional value of fracture toughness (K_Q) has been computed through LEFM approach, as K_{IC} (plane strain fracture toughness), illustrates the crack initiation in linear elastic fracture mechanics. On the other hand, J-integral is another important fracture toughness parameter, illustrates the crack propagation in elastic plastic fracture mechanics [33]. The values of J-integral for the elastic plastic and linear elastic material, respectively, would give the crack propagation and initiation energy according to elastic plastic fracture mechanics [34]. The values of J-integral were evaluated as per the ASTM standard 1820-15a [35, 36] through 3-point bend test data using the following Eq.:

$$J = \frac{2A}{Bb}$$
(6)

where, B is the sample thickness (B=3.75 mm), b is the unbroken ligament (b= 3.75) and A is the area under the load *vs*. displacement curve up the maximum load. J-integral Value was calculated through the Eq. 6 and summarized in Table 3. For example, J-integral value is calculated to be 63.9kJ/m^2 for the multiphase controlled rolled microalloyed steel sample.

Table 3: K_Q, K_{ee} and J-integral values for the microalloyed steel samples subjected to multiphase control rolling.

Processing condition		K_Q (MPa√m)	K_{ee}(MPa√m)	J-integral (kJ/m^2)	Dimple size (μm)
Microalloyed steel	H-AN sample	27.7	32.7	48.78	22
	α+γ phase control rolled sample	46.8	53.4	63.9	12
	Multiphase control rolled sample	53.7	68.9	81.4	6
IF steel	H-AN sample	33.2	36.0	55.6	29
	α-phase control rolled sample	49.3	57.7	69.6	19
	Multiphase control rolled sample	63.5	72.0	87.7	9

It is to be noted that the values of K_Q, K_{ee} and J-integral of the IF and microalloyed steel samples are found to improve after the control rolling as compared to that of the annealed specimens. However, the multiphase control rolled samples showed better improvement in all type of fracture toughness values (K_Q, K_{ee} and J-integral) as compared to that of the other specimens of

the same composition. The improvement of the K_Q, K_{ee} and J-integral is attributed to the formation of submicron size ferrite+martensite structure in the microalloyed steel and ultrafine equiaxed ferrite grains along with high density of dislocation substructures in the IF steel (as shown in Figs. 13a-d). These dislocation cells/substructures could obstruct the initiation and propagation of the crack effectively [32].
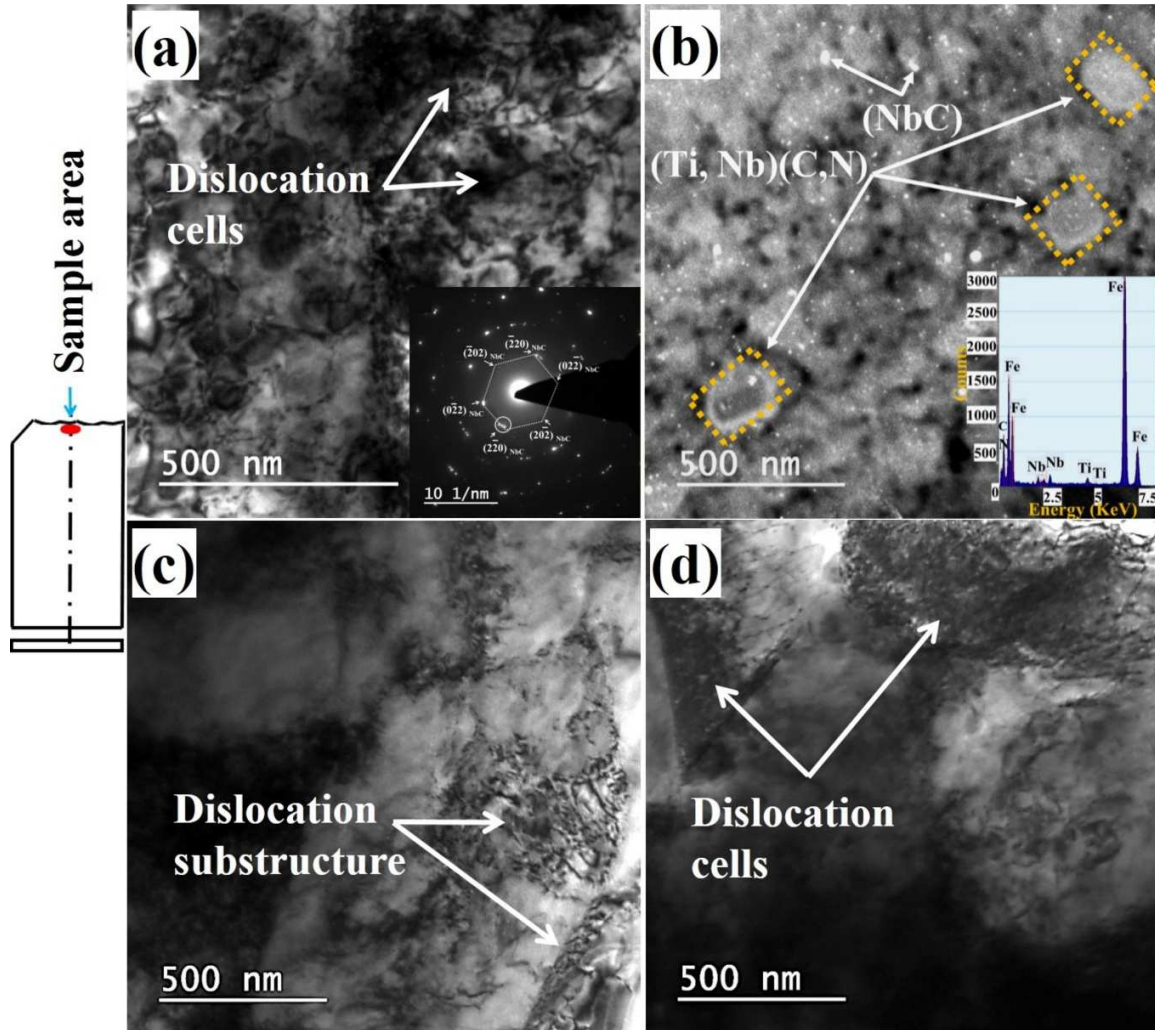

Fig. 13: TEM micrographs of multiphase control rolled (a,b) microalloyed and (c,d) IF steel specimens.

Moreover, a uniformly distributed nanosize niobium carbide (NbC) precipitates (Fig. 13b) is found to form in the microalloyed steel, which could also improve the fracture toughness. Furthermore, Complex cubic shaped Ti-Nb carbonitrides {(Ti,Nb)(C,N)} precipitates are also found to present along with NbC (Fig. 13b). TEM based EDS analysis confirms the existence of cubic shaped (Ti,Nb)(C,N). These carbonitride precipitates may act as heterogeneous nucleation cites for the NbC [37]. Hong et al. [38] observed the formation of NbC precipitates on the

undissolved (Ti,Nb)(C,N) in Nb-Ti microalloyed HSLA steel during double hit deformation at 850-975°C. Baker [37] also observed NbC or Nb(C,N) precipitates nucleation on the (Ti,Nb)N core particles during controlled rolling of 0.1%C steel containing of Nb, Ti and N. He also stated that the presence of Ti and N in the microalloyed steel improved the toughness through pinning of austenite grains by TiN particles during hot deformation.

In the calculation of K_{ee} and J-integral values, both the load as well as area under the curve are considered. On the other hand, only the maximum load is taken care in the calculation of K_Q. Therefore, as compared to the apparent fracture toughness (K_Q) value, the value of fracture toughness parameters i.e. K_{ee} and J-integral are more relevant and valid. Hence, it can be concluded that the multiphase control rolled microalloyed and IF steel specimens exhibited better fracture toughness values than that of the other samples. Similar type of fracture behaviour was also reported by Dashrath et al. [14] and Joshi et al. [15] in the UFG nonferrous materials processed by cryorolling/cryoforging techniques. Enhancement of the fracture toughness in other materials were also investigated by several researchers [39-41] and they have reported that the extensive grain refinement through different SPD methods is the key factor of such improvement. In the present study, the enhancement in the conditional fracture toughness value is ascribed to the development of submicron size ferrite grain, formation of dislocation substructures and precipitation of ultrafine carbides.

3.4 Fractography analysis

Figs. 14a-d show fractographs after the 3-point bend testing of the H-AN, 3-steps multiphase control rolled microalloyed and IF steel specimens. It can be noticed from Figs. 14a and c that the H-AN specimens of both the steels fractured by ductile manner through exposing well-developed larger size dimples (avg. size ~22μm in microalloyed steel and ~29μm in the IF steel) over the entire surface. After the 3-steps multiphase control rolling, the average dimple size decreased to ~6 and 9μm, respectively, in the case of microalloyed and IF steel samples (Figs. 14b and d). The average size of dimples can be associated with the apparent fracture toughness values (Table 3) and the % elongation of the corresponding specimen (Table 2).

Diminishing the size of dimple during multiphase rolling is endorsed to the development of submicron sized ferrite and formation of dislocation sub-cells/substructures. Furthermore, in case

of the microalloyed steel, the presence of cleavage facets can be seen in the fractured surface of the multiphase controlled rolled specimen (Fig. 14b). This is attributed to the presence of hard phase, i.e. martensite (as shown in Fig. 7a) within the soft ferrite matrix. Also, TiN phase may be act as nucleating points for the cleavage in the microalloyed steel. On the other hand, in the IF steel sample, no such hard phase (i.e. martensite) is formed. Furthermore, hardly any TiN precipitates found to be present in the IF steel. Hence, it showed ductile failure. In case of the IF steel, the Nb to Ti stoichiometric ratio is only 0.28. Hence, there may be less possibility of formation TiN precipitates. Moreover, it is also reported that the quantity of Ti (wt.%) essential to tie up with N is 3.42 times (i.e. Ti/N=3.42) [42]. In the analyzed IF steel, N content present around 0.01wt.% only. Thus, the maximum amount of Ti required to tie up with N is 0.0342 wt.%. In the analyzed IF steel, the Ti content is 0.042 wt.% only. Hence, because of the low stoichiometric ratio, there may be little possibility of formation of trace amount of TiN in the IF steel. Many other researchers also [13-15] reported almost similar kinds of fracture behavior for the UFG nonferrous alloys processed through SPD techniques.
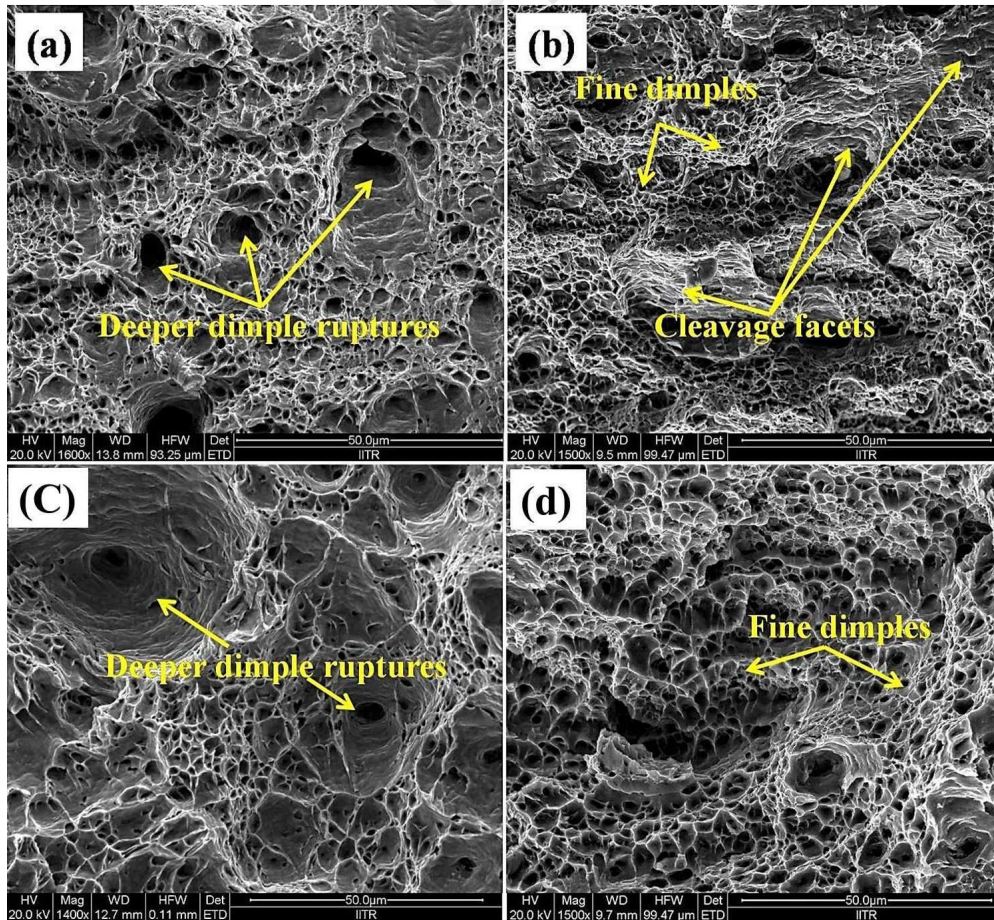
Fig. 14: Fractured surface morphology (a and c) H-AN and (b and d) 3-point bend tested multiphase control rolled microalloyed and IF steel specimens, respectively.

4. Conclusions

Fracture toughness values of the submicron grained IF and microalloyed steel specimens achieved through innovative thermomechanical control processing have been investigated in details and correlated with other mechanical properties. Following conclusions could be the important outcomes of this study.

(i) Innovative 3-steps multiphase rolling has exhibited superior combination of YS and ductility for both the steels i.e. microalloyed (923MPa, 13.5%) as well as IF steel sample (623MPa, 19%) due to evolution of ultrafine grained microstructure (i.e. <1μm). The key mechanism for obtaining such ultrafine grained microstructure (ferrite+martensite with an avg. grain size ~0.69μm in microalloyed and 0.83μm grain size ferritic structure in IF steel) is identified to be the dynamic recrystallization within the deformation induced transformed ferrite under controlled multiphase rolling. On the other hand, single phase control multipass rolling up to 80%RA developed a bimodal grain structures (microalloyed steel: 1-3μm size smaller grain+10-12μm+martensite; IF steel: 1-3μm+elongated ferrite grains with large aspect ratio) and still the maximum grain refinement achieved was ≥1μm.

(ii) The 3-steps multiphase control rolled microalloyed and IF steel specimens showed superior improvement of the fracture toughness (K_{ee}=68.9, 72MPa√m; J=81.4, 87.7kJ/m^2) along with its high YS (923and 623MPa) and significant ductility (13.6 and 19%) as compared to their coarse grained counterparts (K_{ee}=32.7, 36MPa√m; J=48.78, 55.67kJ/m^2). The equivalent energy fracture toughness (K_{ee}) value is highly acceptable as it includes the maximum load as well as area up to the linear extension under 3-point bend test to evaluate its value. On the other hand EPFM approach is also suitable to predict the fracture toughness values as it includes the total area under the load vs. extension curve generated in 3-point bend test. The EPFM concept (J-integral) could interpret crack propagation mechanisms. Both the approaches could predict the realistic fracture toughness values when it is difficult to determine valid K_{IC} of the samples. The improved fracture toughness is attributed to the formation of submicron size

ferrite+martensite structure (avg. size 0.69μm) in the microalloyed steel and ultrafine equiaxed ferrite grains (avg. size 0.83μm) along with high density of dislocation substructures in the IF steel. These dislocation cells/substructures could obstruct the initiation and propagation of the crack effectively.

Overall, the present processing methods, especially, 3-steps multiphase control rolling technique could be highly attractive and novel, which can be used as one of the advanced techniques to produce UFG bulk steels having superior mechanical properties and better fracture toughness. Hence, the processing method could be scale-up for the industrial applications to produce UFG steels for its great technological interest.

Acknowledgement

The authors are thankful to the Metallurgical and Materials Engineering Department, Indian Institute of Technology Roorkee for offering the research facilities to carry out the current research work.

Data availability statement

All data included in this study are available upon request by contacting the corresponding author.

References

[1] W.B. Morrison, Microalloy steels-the beginning, Mater. Sci. Technol. 25 (2009)1066-1073.
[2] R.D.K. Misra, H. Nathani, J.E. Hartmann, F. Siciliano, Microstructural evolution in a new 770 MPa hot rolled Nb-Ti microalloyed steel, Mater. Sci. Eng. A 394 (2005) 339-352.
[3] A. Azushima, R. Kopp, A. Korhonen, D.Y. Yang, F. Micari, G.D. Lahoti, P. Groche, J. Yanagimoto, N. Tsuji, A. Rosochowski, A. Yanagida, Severe plastic deformation (SPD) processes for metals, CIRP Ann. Manuf. Technol. 57 (2008) 716-735.
[4] L.S. Toth, C. Gu, Ultrafine-grain metals by severe plastic deformation, Mater. Charact. 92 (2014) 1-14.
[5] S. Ghosh, A.K. Singh, S Mula, P. Chanda, V.V. Mahashabde, T.K. Roy, Mechanical properties, formability and corrosion resistance of thermomechanically controlled processed Ti-Nb stabilized IF steel, Mater. Sci. Eng. A 684 (2017) 22-36.
[6] S. Ghosh, S. Mula, Thermomechanical processing of low carbon Nb-Ti stabilized microalloyed steel: microstructure and mechanical properties, Mater. Sci. Eng. A 646 (2015) 218-233.
[7] Y.D. Huang, W.Y. Yang, Z.Q. Sun, Formation of ultrafine grained ferrite in low carbon steel by heavy deformation in ferrite or dual phase region, J. Mater. Process. Technol. 134 (2003) 19-25.

[8]   S.C. Hong, K.S. Lee, Influence of deformation induced ferrite transformation on grain refinement of dual phase steel, Mater. Sci. Eng. A 323 (2002) 148-149.

[9]   T. Sakai, A. Belyakov, R. Kaibyshev, H. Miura, J.J. Jonas, Dynamic and post-dynamic recrystallization under hot, cold and severe plastic deformation conditions, Prog. Mater. Sci. 60 (2014) 130-207.

[10] H. Hou, Q. Chen, Q. Liu, H. Dong, Grain refinement of a Nb-Ti microalloyed steel through heavy deformation controlled cooling, J. Mater. Process. Technol. 137 (2003) 173-176.

[11] L. Zhao, N. Park, Y. Tian, S. Chen, A. Shibata, N. Tsuji, Novel thermomechanical processing methods for achieving ultra-grain refinement of low-carbon steel without heavy plastic deformation, Mater. Res. Let. 5 (2017) 61-68.

[12] N. Park, A. Shibata, D. Terada, N. Tsuji, Flow stress analysis for determining the critical condition of dynamic ferrite transformation in 6Ni-0.1C steel, Acta Mater. 61 (2013) 163-173.

[13] A. Hohenwarter, R. Pippan, Fracture toughness evaluation of ultrafine-grained nickel, Scr. Mater. 64 (2011) 982-985.

[14] S.M. Dasharath, S. Mula, Improvement of mechanical properties and fracture toughness of low SFE Cu-Al alloy through microstructural modification by multiaxial cryoforging, Mater. Sci. Eng. A 690 (2017) 393-404.

[15] A. Joshi, N. Kumar, K.K. Yogesha, R. Jayaganthan, S.K. Nath, Mechanical properties and microstructural evolution in Al 2014 alloy processed through multidirectional cryoforging, J. Mater. Eng. Perform. 25 (2016) 3031-3045.

[16] A.I. Toulfatzis, G.A. Pantazopoulos, A.S. Paipetis, Fracture behavior and characterization of lead-free, brass alloys for machining applications, J. Mater. Eng. Perform. 23 (2014) 3193-3206.

[17] S.V.S.N. Murty, S. Torizuka, K. Nagai, T. Kitai, Y. Kogo, Dynamic recrystallization of ferrite during warm deformation of ultrafine grained ultra-low carbon steel, Scr. Mater. 53 (2005) 763-768.

[18] Z.Q. Sun, W.Y. Yang, Q.Q. Ji, Deformation enhanced transformation and dynamic recrystallization of ferrite in a low carbon steel during multipass deformation, Mater. Sci. Eng. A 334 (2002) 201-206.

[19] C.J. Barrett, B. Wilshire, The production of ferritically hot rolled interstitial-free steel on a modern hot strip mill, J. Mater. Process. Technol. 122 (2002) 56-62.

[20] S. Godha, K. Watanabe, Y. Hashimoto, Effects of the intercritical rolling on structure and properties of low carbon steel, ISIJ Trans. 21 (1981) 6-15.

[21] A.D. Paepe, J.C. Herman, V. Leroy, Deep drawable ultra low carbon Ti-IF steels hot rolled in the ferrite region, Steel Res. Int. 68 (1997) 479-486.

[22] E.I. Galindo-Nava, P.E.J. Rivera-Diaz-del-Castillo, Grain size evolution during discontinuous dynamic recrystallization, Scr. Mater. 72-73 (2014) 1-4.

[23] A. Dehghan-manshadi, P.D. Hodgson, Dependency of recrystallization mechanism to the initial grain size, Metall. Mater. Trans. A 39 (2008) 2830-2840.

[24] A. Belyakov, K. Tsuzaki, H. Miura, T. Sakai, Effect of initial microstructures on grain refinement in a stainless steel by large strain deformation, Acta Mater. 51 (2003) 847-861.

[25] CM. Sellars, From trial and error to computer modeling of thermomechanical processing, Ironmak. Steelmak. 38 (2011) 250-257.

[26] T. Gladman, The Physical Metallurgy of Microalloyed Steels, London, The Institute of Material, 1997, pp. 320-380.

[27] R. Song, D. Ponge, D. Raabe, Mechanical properties of an ultrafine grained C-Mn steel processed by warm deformation and annealing, Acta Mater. 53 (2005) 4881-4892.

[28] N. Tsuji, Y. Ito, Y. Saito, Y. Minamino, Strength and ductility of ultrafine grained aluminum and iron produced by ARB and annealing, Scr. Mater. 47 (2002) 893-899.

[29] X. Huang, N. Hansen, N. Tsuji, Hardening by annealing and softening by deformation in nanostructured metals, Science, 312 (2006) 249-251.

[30] G.E. Dieter, Evaluation of workability, Metals Handbook, 9th Edition, 14, American Society of Metals, Metals Park, OH, 1988, pp. 363-372.

[31] E.B. Tochaee, H.R.M. Hosseini, S.M.S. Reihani, On the fracture toughness behavior of in-situ Al-Ti composites produced via mechanical alloying and hot extrusion, J. Alloy. Compd. 681 (2016) 12-21.

[32] X.K. Zhu, J.A. Joyce, Review of fracture toughness (G, K, J, CTOD, CTOA) testing and standardization, Eng. Fract. Mech. 85 (2012) 1-46.

[33] D. Broek, Elementary Engineering Fracture Mechanics, 3rd edition, Springer, Berin, 2012, pp. 24-66.

[34] J.R. Rice, A path independent integral and the approximate analysis of strain concentration by notches and cracks, J. Appl. Mech. 35 (1968) 379-386.

[35] E.E. Gdoutos, Fracture Mechanics: An introduction, 2nd edition, Springer, Berlin, 2006, pp. 1-238.

[36] G.H.B. Donato, C. Ruggieri, Estimation procedures for J and CTOD fracture parameters using three-point bend specimens, Proc. Intern. Pipeline Conf. (2006) 149-157.

[37] T.N. Baker, Microalloyed steels, Ironmaking & Steelmaking. 43 (2016) 264-307.

[38] S.G. Hong, K.B. Kang, C.G. Park, Strain induced precipitation of NbC in Nb and Nb-Ti microalloyed HSLA steels, Scr. Mater. 46 (2002) 163-168.

[39] A. Singh, L. Tang, M. Dao, L. Lu, S. Suresh, Fracture toughness and fatigue crack growth characteristics of nanotwinned copper, Acta Mater. 59 (2011) 2437-2446.

[40] H. Somekawa, T. Mukai, Fracture toughness in ultrafine-grained magnesium alloy, Mater. Sci. Forum. 503 (2006) 155-160.

[41] W. Pachla, M. Kulczyk, J. Smalc-Koziorowska, S. Przybysz, M. Wróblewska, J. Skiba, M. Przybysz, Enhanced strength and toughness in ultra-fine grained 99.9% copper obtained by cryo-hydrostatic extrusion, Mater. Charact. 141 (2018) 375-387.

[42] P. Ghosh, C. Ghosh, R.K. Ray, Precipitation in Interstitial Free High Strength Steels, ISIJ Int. 49 (2009) 1080-1086.

Figure captions

Fig. 1: (a,b) Schematic illustration of the single phase controlled and (c,d) multi-phase controlled rolling schedules for microalloyed and IF steels, respectively.

Fig. 2: (a) Schematic presentation of a 3-point bend specimen, (b) photograph of 3-point bend specimen.

Fig. 3: Optical microstructure of homogenized annealed (a) microalloyed and (b) IF steel specimen.

Fig. 4: (a) Optical microstructure, (b) EBSD inverse pole figure map, (c) grain boundary map of α+γ region control rolled (50% RA) microalloyed steel specimen, (d) misorientation profile of the corresponding microstructure.

Fig. 5: (a) Optical microstructure, (b) EBSD inverse pole figure map, (c) grain boundary map of α+γ region control rolled (80% RA) microalloyed steel specimen, (d) misorientation profile of the corresponding microstructure.

Fig. 6: (a,b) Optical microstructures, (c,d) EBSD inverse pole figure map of α region control rolled 50 and 80%RA IF steel specimens, respectively, (e,f) misorientation profile of corresponding specimens, respectively.

Fig. 7: Optical microstructures of 3-steps multi-phase control rolled (a) microalloyed and (b) IF steel as per designed schedule, respectively.

Fig. 8: (a) EBSD inverse pole figure and (b) grain boundary maps of 3-steps multi-phase control rolled microalloyed steel as per designed schedule; (c,d) Misorientation profile and grain size distribution of corresponding specimen, respectively.

Fig. 9: (a) EBSD inverse pole figure and (b) grain boundary maps of 3-steps multi-phase control rolled IF steel as per designed schedule; (c,d) Misorientation profile and grain size distribution of corresponding specimen, respectively.

Fig. 10: TEM bright field image of 3-steps multi-phase control rolled (a) microalloyed and (b) IF steel as per innovative designed schedule.

Fig. 11: Tensile stress-strain curves of TMCRed (a) microalloyed and (b) IF steel specimens.

Fig. 12: (a) Representative load *vs*. extension plot for the α+γ phase control microalloyed steel sample to calculate the equivalent load, P_E, used to evaluate equivalent fracture toughness, K_{ee}, (b,c) Load *vs*. extension curves of microalloyed and IF steel specimens rolled in different processing conditions, respectively.

Fig. 13: TEM micrographs of multiphase control rolled (a,b) microalloyed and (c,d) IF steel specimens.

Fig. 14: Fractured surface morphology (a and c) H-AN and (b and d) 3-point bend tested multiphase control rolled microalloyed and IF steel specimens, respectively.

Table captions

Table 1: Chemical composition (wt. %) of the low C microalloyed and IF steels.

Table 2: The Mechanical properties of the Homogenized annealed (H-AN) and TMCRed microalloyed and IF steel specimens.

Table 3: K_Q, K_{ee} and *J*-integral values for the microalloyed steel samples subjected to multiphase control rolling.

Research Highlights

- UFG microalloyed and IF steels have been produced through innovative multiphase control rolling.

- Formation of UFG microstructure has been analyzed in the light of deformation DIFT/DRX mechanisms.

- Analyzed the fracture toughness through computing K_Q, J-integral and K_{ee} values from 3-point bend test.

- Quantitative measurements of low/high angle grain boundaries were determined through EBSD/TEM analysis.

- High fraction of dislocation cells/substructures could effectively block the crack initiation/propagation.

Declaration of interests

☒ The authors declare that they have no known competing financial interests or personal relationships that could have appeared to influence the work reported in this paper.